Balthazar *et al.*
International Journal of Air-Conditioning and Refrigeration (2026) 34:16
https://doi.org/10.1007/s44189-026-00107-4

International Journal of
Air-Conditioning and Refrigeration

RESEARCH Open Access

Performance analysis of a Brayton Barocaloric refrigeration cycle using $(C_9H_{19}NH_3)_2CuBr_4$ as refrigerant

Pravinth Balthazar[1*], Mohammad S. Islam[1] and Nick S. Bennett[1]

Abstract
Barocaloric materials promise eco-friendly alternatives to vapour compression in refrigeration, with $(C_9H_{19}NH_3)_2CuBr_4$ being a focus of this study. It is a highly promising barocaloric refrigerant due to the 0.4 K hysteresis temperature and operational pressure as low as 500 Bar. A reversible and irreversible Brayton Barocaloric refrigeration cycle analysis is established. For the irreversible cycle, the irreversibility during the compression and expansion process is considered in the two adiabatic processes. Performance characteristics are investigated across various indoor and outdoor temperature ranges, material operational temperature points, and operating pressures to determine the Coefficient of Performance (COP) and Dimensionless Refrigeration Capacity (DRC). The guidance for optimising the irreversible Brayton Barocaloric refrigeration cycle analysis is provided by disclosing the impact of the irreversibility of work process efficiency, timing ratio, and heat reservoir temperatures. Moreover, several specific cases are examined in detail. The results demonstrate that maximising the phase transition region of $(C_9H_{19}NH_3)_2CuBr_4$ results in a COP of 10.8 achieved at a temperature span of 3.5 K while maintaining a 0.9-time ratio and conservative irreversibility efficiency of 0.8. This material is capable of cooling by 5.0 K with a reasonable COP of 2.5 at the 0.75-time ratio for a heat source temperature of 309 K and heat sink temperature of 314 K. Finally, this study demonstrates the potential for constructing a simple Barocaloric refrigeration system to validate the concept, with opportunities for further improvement through modifications.

Keywords Barocaloric materials, Brayton refrigeration cycle, Irreversibility, COP, Dimensionless Refrigeration Capacity

1 Introduction

Global warming is a critical global concern, with combined surface air and sea surface temperatures rising by approximately 1.0 °C since the pre-industrial era, at a rate of about 0.2 °C per decade [1]. While the primary focus in the 1990s was the adoption of refrigerants with zero ozone depletion potential (ODP), current efforts emphasise the transition toward alternative cooling technologies with low global warming potential (GWP) and the development of high-efficiency systems [2]. This shift aims to reduce the direct environmental impact of refrigerants and the indirect emissions from energy consumption. One significant factor contributing to global warming is the role of refrigeration, which constitutes approximately 7.8% of the total global greenhouse gas emissions. A significant 63% of these emissions come from "indirect" sources. This underlines the importance of focusing on sustainable solutions in the refrigeration sector to reduce environmental impact [3]. As a large share of global electricity is generated from fossil fuels,

*Correspondence:
Pravinth Balthazar
Pravinth.Balthazar@uts.edu.au
[1]School of Mechanical and Mechatronic Engineering, University of Technology Sydney, Ultimo, NSW 2007, Australia

Springer

improving the efficiency is also essential to lowering their overall climate impact.

Steven Brown and Domanski extensively assessed 'not in kind' technologies as alternatives to vapour compression cooling (VCC) technologies [4]. They evaluated eighteen cooling technologies with the potential to partially or fully replace VCC systems within the next two decades and concluded that caloric cooling technologies could achieve exergy efficiencies of up to 60%, significantly higher than other alternatives. Additionally, caloric refrigeration technologies employing solid refrigerants are appealing due to their eco-conscious nature and zero direct GWP. Barocaloric refrigeration reduces environmental impact by utilising solid-state materials instead of harmful gases, thereby avoiding direct greenhouse gas emissions. These technologies hold strong potential for applications in residential refrigeration, HVAC systems, data centres, and industrial process cooling. Aprea et al. (2023) demonstrated through a two-dimensional numerical analysis using the Total Equivalent Warming Impact (TEWI) method that Active Barocaloric Refrigeration reduces environmental impact by up to 58% compared to conventional vapour compression systems [5]. The use of nanofluids as heat transfer fluids further enhances this reduction to 62%.

Barocaloric cooling recently gained renewed attention, driven by the discovery of Neopentyl glycol (NPG). It has a first-order phase transition temperature (T_{tr}) of 315 K and exhibits a Barocaloric effect of 421 J K^{-1} kg^{-1}, comparable to those of the hydrofluorocarbon (HFC) R-134a. However, NPG faces two significant challenges: significant hysteresis up to 24 K and the need for high barocaloric pressures, ranging from 200 to 570 MPa [6, 7]. In their 2022 study, Seo et al. examined $(NA)_2CuBr_4$, metal-halide perovskites, with NA representing nonyl ammonium ($C_9H_{19}NH_3$) [8]. The research revealed the material's efficient operation under low hydrostatic pressure and significant pressure-sensitive order–disorder phase transitions. Notably, its operational pressure of 50 MPa is five to ten times smaller than that of NPG. Compared to NPG, $(NA)_2CuBr_4$ is the most promising material that exhibits first-order phase transition temperatures (T_{tr}) closer to room temperature, making it more practical, with a transition temperature of 305.5 K, approximately 10 K lower than NPG. This characteristic makes $(NA)_2CuBr_4$ well-suited for diverse applications in IT equipment and data centres across all ranges, from A1 to A4 [9]. Additionally, $(NA)_2CuBr_4$ demonstrates minimal hysteresis temperatures as small as 0.4 K [8].

For a comprehensive overview of barocaloric materials and their performance, readers are referred to [10–13], which provide extensive reviews. Kitanovski et al. [10] reviewed caloric materials, including barocaloric systems, their classifications, and conceptual device designs. Plovers et al. [12], summarised key milestones, with emphasis on giant barocaloric effects, and analysed material trade-offs among parameters such as transition temperature (Tr), its pressure dependence (dT/dp), thermal conductivity, refrigeration capacity, operating pressure, density, effect magnitude, and hysteresis. Cirillo et al. [13] classified materials based on structural composition and examined barocaloric refrigeration systems across various potential thermodynamic cycles, including their operation and numerical modelling. Qian et al. [11] comprehensively reviewed elastocaloric cooling, a mechanocaloric technology closely related to barocaloric systems. Their work presents fundamental and advanced thermodynamic cycles, drawing on analogies with other solid-state cooling technologies, and provides a foundation and key insights for the development and analysis of barocaloric thermodynamic cycles. Although numerous researchers have focused on discovering materials exhibiting colossal Barocaloric effects, there has been extremely limited exploration of the refrigeration cycle involving Barocaloric materials.

Dai et al. conducted thermodynamic cycle analyses to assess the performance of the Barocaloric system, utilising NPG as the refrigerant [14]. They concluded that the Coefficient of Performance (COP) for the Barocaloric refrigeration system based on NPG could theoretically attain a maximum value of 8.8. In practical terms, a COP of 3 can be achieved with a temperature span of 10 K when the system operates at room temperature. Recently, a few researchers have explored alternative directions in barocaloric refrigeration studies by conducting molecular dynamics simulations for NPG [15], enhancing its thermal conductivity, and shifting its solid–solid phase transition closer to room temperature [16, 17]. Dai et al. (2024) developed a one-dimensional dynamic model using NPG for a Brayton Barocaloric refrigeration cycle and demonstrated a maximum COP of 13.1 and a refrigeration capacity of 106.4 W at a 10 K temperature span under a 570 MPa cycle [15]. Similarly, Qian et al. (2024) performed a molecular dynamics analysis based on a reversed Stirling cycle and reported a COP of 14 at a 5 K temperature span [18].

However, comprehensive studies on barocaloric refrigeration cycles remain limited, particularly for $(NA)_2CuBr_4$. Therefore, this paper explores the impact of different Barocaloric pressures, indoor and outdoor temperatures, material's operational compression and expansion points, efficiency of compression and expansion process and time ratio (t_r) on the dimensionless refrigeration capacity (DRC) and COP of the Brayton Barocaloric refrigeration cycle for $(NA)_2CuBr_4$. Thermodynamic equations and cycle analysis were employed using computer simulations to investigate the system's performance and operating characteristics. This study also sets

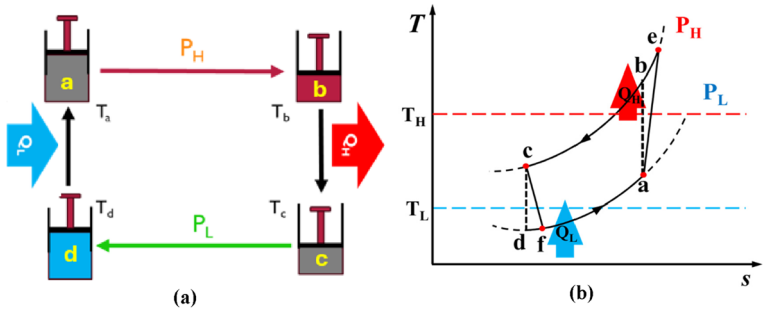

Fig. 1 Four steps of a Brayton barocaloric refrigeration device (**a**) and operation of a barocaloric refrigeration cycle (**b**)

the stage for assessing the material's potential for future studies, paving the way for developing a proof-of-concept device using $(NA)_2CuBr_4$.

2 Methodology

2.1 Illustration of the barocaloric refrigeration system

A simple operation of a Barocaloric refrigeration system is demonstrated in Fig. 1a. This systematic process unfolds in four stages: during the adiabatic compression stages a to b, pressure is raised from P_L to P_H, leading to a volume reduction and temperature elevation. It is assumed that, under uniaxial loading, a uniform phase transformation occurs throughout the material simultaneously for all the thermodynamic processes. The subsequent stage, isobaric enthalpy transfer, includes heat transfer from the material to the surroundings in stages b to c. Adiabatic expansion reduces pressure from P_H to P_L, wherein the hydrostatic pressure is removed. This results in volume expansion and temperature decrease between stages c and d. The final stage involves isobaric entropy transfer processes, where heat is absorbed from the surroundings to the material, maintaining high entropy from stages d to a.

2.2 A barocaloric Brayton refrigeration cycle of $(NA)_2CuBr_4$

The Brayton refrigeration cycle involves the integration of two adiabatic and two isobaric processes, as illustrated in Fig. 1b. The temperatures T_a, T_b, T_c, T_d, T_e, and T_f are marked and labelled at state points a, b, c, d, e and f, respectively. The adiabatic processes a–b and c–d are reversible, while processes a–e and c–f are irreversible. The adiabatic compression and expansion processes are implemented within thermally anhysteretic regions, a phenomenon validated in previous studies [19, 20]. P_L and P_H denote the hydrostatic pressures in the isobaric pressure processes d = > a or f = > a and e = > c or b = > c, respectively, depending on the irreversible or reversible cycle. Q_H and Q_L represent the heat exchanged between the Barocaloric material and the heat reservoirs at temperatures T_H (heat sink) and T_L (heat source) per cycle. The temperature difference between the heat sink and heat source is referred to as the temperature span of the Barocaloric refrigeration system.

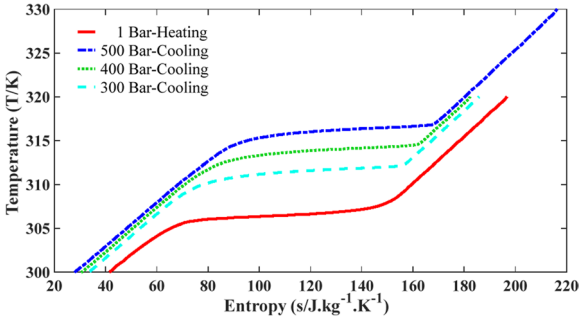

Fig. 2 T-S diagram of $(NA)_2CuBr_4$ for a heating process at 1 Bar and cooling process at 300, 400 and 500 Bar

2.3 Development of a metastable temperature-entropy diagram for $(NA)_2CuBr_4$

In the current study, the material properties investigated by Seo et al. (2022) were employed to establish the metastable temperature-entropy (*T-S*) diagram for $(NA)_2CuBr_4$ near the phase transition region [8]. The temperature-entropy data were extracted from the original publication by Seo et al. (2022) and its supplementary material (Supplementary Fig. 22) [8], enabling reproduction of the *T-S* diagram shown in Fig. 2. Subsequently, the reconstructed dataset was implemented in MATLAB as numerical temperature-entropy relationships, enabling both analytical representation and graphical reconstruction of the diagram. These formulations were then employed to analyse the thermodynamic cycle of $(NA)_2CuBr_4$. The practical implementation of a Barocaloric cycle involves both irreversible and reversible 'material' processes. Irreversible Barocaloric material processes occur during the initial application of pressure to the material, transitioning from a low-pressure and low-temperature state to a high-pressure and high-temperature state. Conversely, reversible Barocaloric material processes operate between a low-pressure and high-temperature state and a high-pressure and low-temperature state. To implement this, a reverse Brayton cycle (Brayton Refrigeration cycle) was developed using

the cooling *T(S)p* curve at high pressure and the heating *T(S)p* curve at atmospheric pressure. It is essential to note that Stern-Taulats et al.'s evidence confirms the reproducibility of entropy change in Barocaloric effects upon field cycling [19, 20]. Based on the literature, the reversibility of the Barocaloric effect induced by pressure changes in thermally anhysteretic regions has been validated, along with the application of *T-S* diagrams for analysing the performance of Barocaloric materials [14]. Therefore, regions bounded by *T-S* ($p = 1$ Bar) on heating and *T-S* ($p = 300$ Bar), *T-S* ($p = 400$ Bar), and *T-S* ($p = 500$ Bar) on cooling are considered reversible, as demonstrated in Fig. 2. Additionally, it is assumed that the material properties remain constant within the small temperature range of interest.

In the specified Barocaloric refrigeration cycle, Fig. 1b, the heat transferred during the two isobaric processes is represented as follows:

$$Q_H = k_1 (LMTD)_H t_1 \tag{1}$$

$$Q_L = k_2 (LMTD)_L t_2 \tag{2}$$

Q_H is the amount of heat rejected from the material to the heat sink, and Q_L is the amount of heat absorbed by the material from the heat source. In the equation, k_1 and k_2 represent the thermal conductance between the cyclic working substance and the heat reservoirs at temperatures, respectively, at outdoor temperature (T_H) and indoor temperature (T_L), while t_1 and t_2 indicate the corresponding heat exchange times. Combining insights from prior studies on magnetic refrigeration [21–23], $(LMTD)_L$ and $(LMTD)_H$ are characterised as the average temperature difference between the heat source or heat sink and the barocaloric material housed within the cylinder. Temperatures T_i and T_j denote the material's temperature after the adiabatic compression and expansion process, respectively. If the barocaloric refrigeration cycle is reversible ($\eta = 1$), temperatures T_i and T_j appear as T_b and T_d in the logarithmic heat transfer model. However, if the cycle is irreversible, the temperatures would be T_e and T_f.

$$(LMTD)_H = \frac{(T_i - T_H) - (T_c - T_H)}{\ln\{(T_i - T_H)/(T_c - T_H)\}} \tag{3}$$

$$(LMTD)_L = \frac{(T_L - T_j) - (T_L - T_a)}{\ln\{(T_L - T_j)/(T_L - T_a)\}} \tag{4}$$

The coefficient of performance (COP_L) of refrigeration is defined as the ratio of useful cooling output to the compression work input of the barocaloric system, as given in Eq. 5. Neglecting the heat loss during the heat transfer process, the work done by piston cylinders can be written as $W = Q_H - Q_L$.

$$COP_L = \frac{Q_L}{W} = \frac{Q_L}{Q_H - Q_L} \tag{5}$$

In evaluating the performance of a refrigeration system, crucial indicators include refrigeration capacity *(RC)* and coefficient of performance (*COP*). These factors are essential to uncover optimal characteristics and examine the influence of indoor and outdoor temperatures on refrigerator performance. The duration of adiabatic processes is significantly shorter than that of isobaric processes, allowing us to neglect the adiabatic process time. Consequently, the cycle period for the refrigerator is approximately equal to the sum of t_1 and t_2 ($t = t_1 + t_2$).

$$RC = \frac{Q_L}{t} \tag{6}$$

Dimensionless refrigeration capacity (*DRC*) is introduced to analyse the performance of barocaloric material by enabling comparison independent of the operating temperature scale. Two cases are proposed for the analysis of the *DRC*.

$$DRC_1 = \frac{RC}{kT_L} \tag{7}$$

Case 1 (DRC_1), the assumption is that thermal conductance between the barocaloric material contained cylinder and the heat reservoirs k_1 and k_2 are equal (k), and the time taken for heat exchange during both isobaric conditions are equal ($t_1 = t_2$). In Case 2 (DRC_2), the assumption is that thermal conductance k_1 and k_2 are equal (k), but the time taken for both heat exchanges is not equal ($t_1 \neq t_2$). Therefore, the time ratio (t_r) is introduced to optimise the irreversible Brayton barocaloric refrigeration cycle to maximise the *COP* and *DRC*. The time ratio refers to the duration during which the exothermic process (t_1) rejects heat to the outdoor environment (acting as a heat sink), and the endothermic (t_2) process absorbs heat from the indoor environment (acting as a heat source). This time ratio can be adjusted by the barocaloric refrigeration device to optimise the system's performance.

In terms of real-world operation, the timing ratio can be interpreted as follows, based on the barocaloric cycle operation using a piston–cylinder system coupled to external heat reservoirs. Following compression, heat is rejected to the hot reservoir while the piston maintains the applied pressure, and work input continues during this stage. In contrast, after expansion, the piston remains stationary, and no further work input is required.

Accordingly, a timing ratio is introduced to define the distribution of cycle time allocated to heat exchange with the external reservoirs. This parameter is used to capture the balance between isobaric enthalpy transfer and isobaric entropy transfer process durations, thereby governing the trade-off between adiabatic temperature change, heat transfer effectiveness, and overall system performance.

$$t_r = \frac{t_1}{t_2} \tag{8}$$

Our study developed a heat transfer model to calculate the Dimensionless Refrigeration Capacity of the DRC_2 system under different isobaric enthalpy transfer processes after compression and expansion. This model was inspired by the research of Yang et al., 2020 and Xia et al., 2008, aiming to analyse the heat exchange time between the working substance and the heat sink and heat source [24, 25]. Hence, both compression and expansion are adiabatic processes. The compressibility factor of the compression (β_1) and expansion (β_2) are assumed to be equal (β) during the reversible barocaloric refrigeration cycles and unequal during the irreversible cycle.

$$\beta_2 = \frac{T_c}{T_d} \tag{9a}$$

$$\beta_1 = \frac{T_b}{T_a} \tag{9b}$$

This research emphasises the influence of the temperature difference in heat transfer on the system performance. Consequently, the impact of thermal conductance on the system performance is disregarded. For the reversible cycle, the compression and expansion processes are isentropic, and it is assumed that the spacing ratio between the pressure curves P_H and P_L remains the same, similar to the magnetocaloric curve [25]. Dimensionless Refrigeration Capacity and *COP* are defined using Eqs. 2, 5, 6, 7, 9a and $t_1 = t_2$ as,

$$DRC = \frac{RC}{kT_L} = \frac{(LMTD)_H * (LMTD)_L}{[\beta_2 (LMTD)_L + (LMTD)_H] * T_L} \tag{10a}$$

$$COP = \frac{(LMTD)_L}{(LMTD)_H - (LMTD)_L} \tag{10b}$$

Irreversibility during compression and expansion arises from non-ideal piston–cylinder behaviour, including mechanical losses and internal friction. As a result, the actual thermodynamic paths deviate from the ideal isentropic processes. To quantify these effects, compression and expansion efficiencies are introduced to relate the actual temperature (or entropy) change to the corresponding ideal isentropic change. Incorporating such irreversibilities is essential in the numerical model, as it enables more realistic predictions of cycle performance, including *COP*, *DRC*, and cooling temperature span. Accordingly, compression and expansion efficiencies are defined in Eqs. 11a and 11b for the irreversible barocaloric refrigeration cycle.

$$\eta_c = \frac{T_b - T_a}{T_e - T_a} \tag{11a}$$

$$\eta_e = \frac{T_c - T_d}{T_c - T_f} \tag{11b}$$

The optimisation equation for *COP* and *DRC*, based on the time ratio for the irreversible cycle and a logarithmic heat transfer model, was developed and is defined in Eqs. 12a and 12b.

$$DRC = \frac{(LMTD)_L}{(1 + t_r) T_L} \tag{12a}$$

$$COP = \frac{(LMTD)_L}{t_r (LMTD)_H - (LMTD)_L} \tag{12b}$$

For the irreversible cycle, Eqs. 12a and 12b for *COP* and *DRC* can be further simplified using Eqs. 3, 4, 8, 9a and 9b, 10a and 10b, and 11a–11b, and $t_1 \neq t_2$ are expressed as follows in Eqs. 13a and 13b,

$$DRC = \frac{[\beta_2 T_\alpha - \{(\eta_e \{1 - \beta_2\} + \beta_2) T_c\}]}{\beta_2 \ln(u) (1 + t_r) T_L} \tag{13a}$$

$$COP = \frac{1}{t_r \left\{ \frac{\beta_2 \ln(u [\{\eta_c + (\beta_1 - 1)\} T_\alpha - T_c \eta_c])}{\eta_c \ln(v) [\beta_2 T_\alpha - \{(\eta_e \{1 - \beta_2\} + \beta_2) T_c\}]} \right\} - 1} \tag{13b}$$

where,

$$v = \frac{[\eta_c + \{(\beta_1 + 1) T_a\}] - \eta_c T_H}{\eta_c \{T_c - T_H\}}$$

$$u = \frac{(T_L \beta_2) - \{\beta_2 + \eta_e (1 - \beta_2) T_c\}}{\beta_2 (T_L - T_a)}$$

Equations 13a and 13b indicate that the adiabatic irreversibility factors (η_c and η_e), the operating temperature points (T_a and T_c), the heat reservoir temperatures (T_H and T_L), and the timing ratio (t_r) are key parameters governing the performance of the irreversible BBR cycle. Therefore, a comprehensive analysis of their influence on

Table 1 Summary of operational parameters used in the study for the reversible cycle

Barocaloric Pressure Cycle (Bar)	Work Process Efficiency—(η)	Indoor Temperature Range (K)—T_L	Outdoor Temperature Range (K)—T_H	Compression Operational Temperature Range (K)—T_a	Expansion Operational Temperature Range (K)—T_c
300 Bar to 1 Bar 400 Bar to 1 Bar 500 Bar to 1 Bar	1.00	308.50–311.50	308.50–314.50	306.80–308.40	314.30–316.10

Table 2 Summary of operational parameters used in the study for the irreversible cycle

Barocaloric Pressure Cycle (Bar)	Work Process Efficiency -(η)	Indoor Temperature Range (K)—T_L	Outdoor Temperature Range (K)—T_H	Compression Operational Temperature Range (K)—T_a	Expansion Operational Temperature Range (K)—T_c	Timing ratio—t_r
500 Bar to 1 Bar	0.40–1.00	308.50–311.50	308.50–314.50	306.80–308.40	314.30–316.10	0.10–2.50

optimal performance characteristics is required. Thus, MATLAB 2023(a) was used to compile code to generate results based on these expressions, and the *T-S* diagram developed in MATLAB, shown in Fig. 2, was utilised for analysis and optimisation in this study.

3 Results and discussion

The minimum pressure essential for a reversible adiabatic temperature change ($p_{rev,\ ad}$) of $(NA)_2CuBr_4$ is set at 148 Bar. This pressure is critical for demonstrating effective cooling performance within the Brayton refrigeration cycle. The formulas presented in the methodology section are applied to calculate *COP* and *DRC* for both reversible and irreversible Brayton Barocaloric Refrigeration cycles. These formulas are applied by modifying the temperature differences of heat transfer within the specified operating temperature range. Sections 3.1 to 3.3 discuss the reversible Brayton Barocaloric Refrigeration cycle (Ideal BBR cycle), while Sects. 3.4 and 3.5 cover the irreversible Brayton Barocaloric Refrigeration cycle.

Tables 1 and 2 summarise operation parameters used in the reversible and irreversible thermodynamic cycle analysis to provide clarity on the scope and range of the parameters investigated in this study. This includes the barocaloric pressure cycles, work process efficiency range, indoor and outdoor temperature ranges, operational temperature ranges during compression and expansion, and the timing ratio. The indoor and outdoor temperature ranges were selected based on the phase transition behaviour of $(NA)_2CuBr_4$, which transforms from the triclinic (TC) to the orthorhombic (OH) phase while absorbing heat at approximately 305.5 K under 1 bar and reverts back to the TC phase while rejecting heat at around 316.5 K under 500 Bar [8]. The transition temperatures for the 300 Bar and 400 Bar cycles fall within this range.

3.1 The impact of operational pressure

Operational pressures of 300 Bar, 400 Bar, and 500 Bar are specifically examined based on $(NA)_2CuBr_4$'s *T-S* diagram to understand their respective impacts on the Barocaloric system's performance in an Ideal BBR cycle. Operational points are selected based on the system's full utilisation in the phase transition region for this analysis, where the compression (T_a) and expansion (T_c) temperatures are 308.37 K and 314.3 K, respectively (entropy 90 and 150 $JKg^{-1}\ K^{-1}$). This investigation includes the heat reservoir temperature range of T_L—308.5 K to 311.5 K and T_H—308 K to 314 K.

Figure 3a and b display the DRC_2 considering not equal heat exchange times during both isobaric conditions and COP_2 variation with outdoor temperatures at hydrostatic pressures: 300, 400, and 500 Bar, while Fig. 4a and b respectively demonstrate the same trends for indoor temperatures under identical conditions. The DRC_2 shows an increase with the rise in operational pressure, regardless of operating temperature conditions. This occurrence is attributed to the fact that higher pressure induces a more significant first-order chain melting in Barocaloric materials, resulting in an enhanced capacity for heat absorption and rejection. The Barocaloric cycle operated at 500 Bar exhibited 8.6% and 25.6% higher DRC_2 compared to 400 Bar and 300 Bar, respectively, under outdoor temperature conditions of 309.0 K in Fig. 4b. On average, operating at 500 Bar yields 22.8% and 42.6% higher overall DRC_2 compared to operation at 400 Bar and 300 Bar, respectively.

In addition to higher refrigeration capacity, operating at 300 Bar provides an indoor cooling temperature span of only 1 K and an outdoor operating temperature span of 2.25 K. This limited cooling temperature span is the main reason why Fig. 3 does not present the material's performance at an indoor temperature of 309.5 K under 300 Bar. At 400 Bar, the indoor span increases to 1.75 K and the outdoor span to 3.75 K. In contrast, operating at 500 Bar enables indoor cooling of 2.75 K

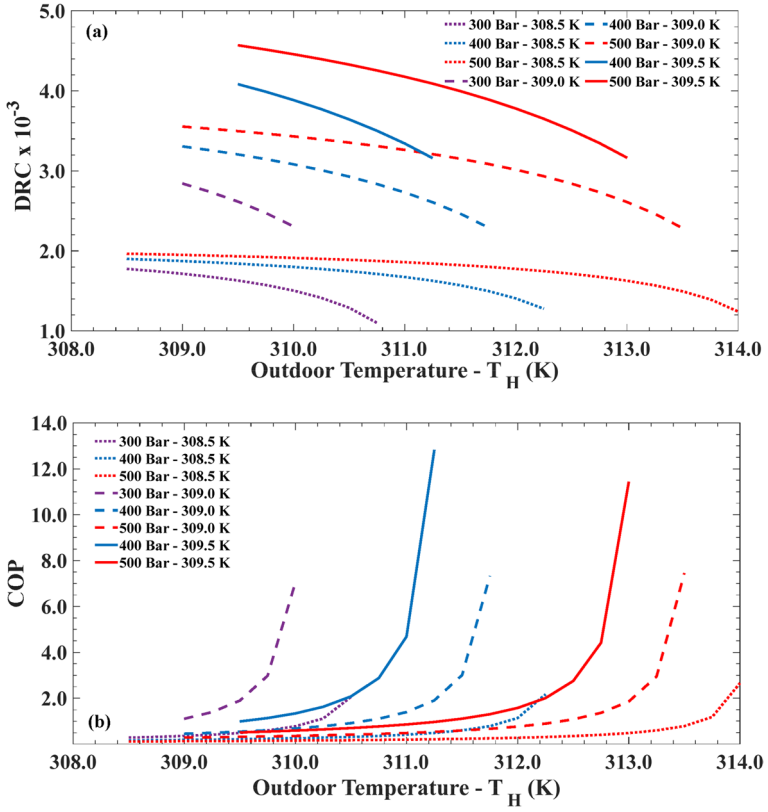

Fig. 3 Comparison of DRC (3**a**) and COP (3**b**) under various outdoor temperatures

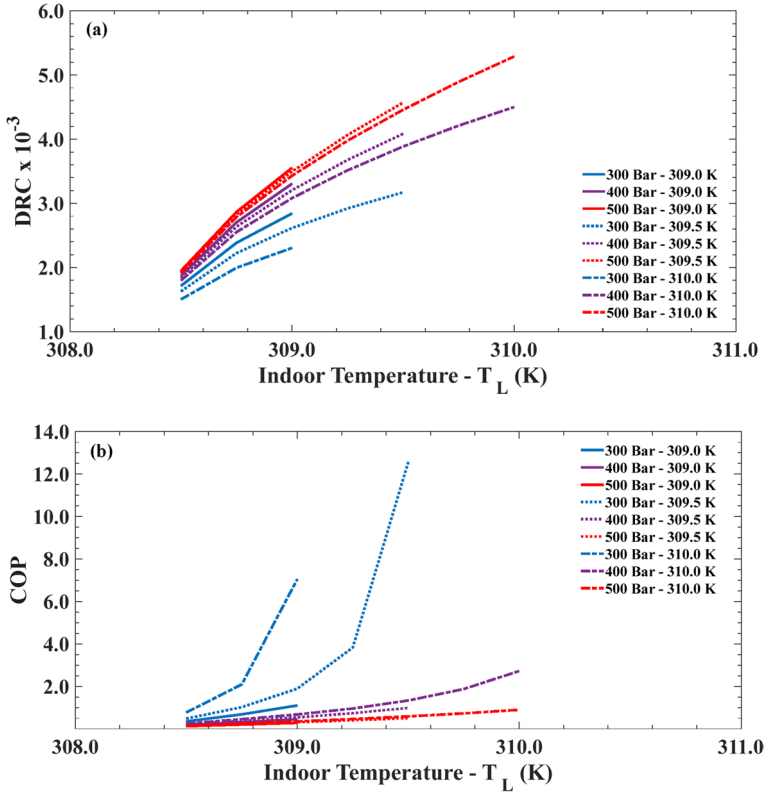

Fig. 4 Comparison of DRC (4**a**) and COP (4**b**) under various indoor temperatures

and an outdoor span of 6.5 K. However, when the outdoor temperature increases at a constant indoor temperature, the DRC_2 of the cycle with lower operating pressure in Fig. 3a decreases rapidly, while the variation trend of DRC_2 under 400 and 500 Bar operating pressures decreases gradually. The opposite trend is observed when the indoor temperature elevates at a constant outdoor temperature, irrespective of the Barocaloric pressure cycle. The reason for the latter is that, as room temperature increases, the material's transition from the triclinic (TC) to the orthorhombic (OH) phase occurs near the upper end of the orthorhombic phase spectrum. Therefore, a greater amount of heat energy must be dissipated to return the material to its triclinic phase. Consequently, the system's refrigeration capacity increases, leading to a greater improvement in *DRC*.

The material demonstrates that, regardless of barocaloric pressure, the COP_2 increases significantly with rising indoor and outdoor temperatures. This increase is attributed to reduced work input at higher indoor temperatures; less work is needed to lower the temperature by 0.1 K compared to 1 K. Similarly, when indoor temperature is constant and outdoor temperature increases, the reduced temperature gradient between the material and the heat sink allows the material to reach the outdoor temperature more quickly. This shortens the heat rejection time, reduces the duration of high-pressure application, and ultimately lowers the system's work input, leading to a higher COP_2.

Additionally, lower barocaloric pressures consistently yield higher COP values throughout the analysis. Using the operating region of 300 Bar as a reference, at 308.50 K, it exhibits 22.3% and 36.5% higher COP_2 compared to 400 Bar and 500 Bar, respectively. At 500 Bar, COP_2 is lower than at 400 Bar and 300 Bar for both heat sink and source temperatures, indicating higher work requirements for material compression compared to the energy extracted from the heat source. Although inefficient in some scenarios, this is inevitable due to the expanded temperature span for refrigeration within the cycle with increased operational pressure. Under high barocaloric pressure, the material releases a substantial amount of energy in a short time, leading to elevated heat rejection temperatures. This enables operation under higher outdoor temperature conditions compared to lower-pressure cycles. As a result, operating at higher pressures extends the cooling temperature span. Furthermore, the increased energy rejection at higher pressures enhances the material's refrigeration capacity. Consequently, an ideal Barocaloric refrigeration cycle operating at 500 Bar is selected for further study in the next sections from 3.2 to 3.5, due to its high-temperature cooling span and *DRC*.

The cyclic application of 500 Bar to the solid-state refrigerant presents practical implementation challenges within a piston–cylinder-based barocaloric system. Such high-pressure operation necessitates mechanically robust components and high-integrity sealing capable of withstanding repeated pressurisation cycles. Materials such as stainless steel, titanium alloys, and hardened tool steels are suitable candidates due to their superior strength and fatigue resistance. Moreover, precise synchronisation of compression and expansion is essential to maintain cycle efficiency. With appropriate mechanical design and control strategies, a prototype system can be developed and experimentally validated under laboratory conditions, supporting the numerical findings presented in Sects. 3.2 to 3.5.

3.2 The impact of heat reservoir temperatures at 500 bar cycle

The relationship of *DRC* with outdoor (T_H) and indoor (T_L) and the combination of indoor and outdoor temperatures is illustrated in Fig. 5a, b and c, respectively. The DRC_2 exhibits an inverse relationship with outdoor temperatures across all operating pressures while demonstrating a direct proportionality with indoor temperatures. If the outdoor temperature (T_H) remains constant, the energy rejected (Q_H) by the barocaloric material remains steady. An increase in indoor temperature (T_L) reduces the temperature span (ΔT), making it easier for the system to extract heat from the indoor environment, and more energy is absorbed (Q_L) from the heat source. In contrast, if the indoor temperature remains constant while the outdoor temperature increases, the ΔT also increases. The barocaloric system will be required to work harder to emit heat, and minimal energy will be rejected during the exothermic process due to the smaller temperature difference between barocaloric materials and the outdoor environment.

Four cases (A–D) were selected to analyse and compare the *COP* and *DRC* performance of the material using indoor–outdoor temperature contour maps. These cases are indicated in Fig. 5c and d, and the corresponding temperature combinations are summarised in Table 3. The cases represent a broad range of operating conditions. Case A corresponds to the widest cooling temperature span. Cases B and D share the same indoor temperature, with Case B representing the highest feasible outdoor temperature at 312.5 K. Case C has the same outdoor temperature as Case D but has a different indoor temperature. This selection ensures a representative comparison for evaluating the effects of indoor and outdoor temperatures on *COP*, *DRC*, and the achievable temperature span.

The lower-right regions in Fig. 5c and d, labelled "Undefined Region," indicate that the *COP* is not defined

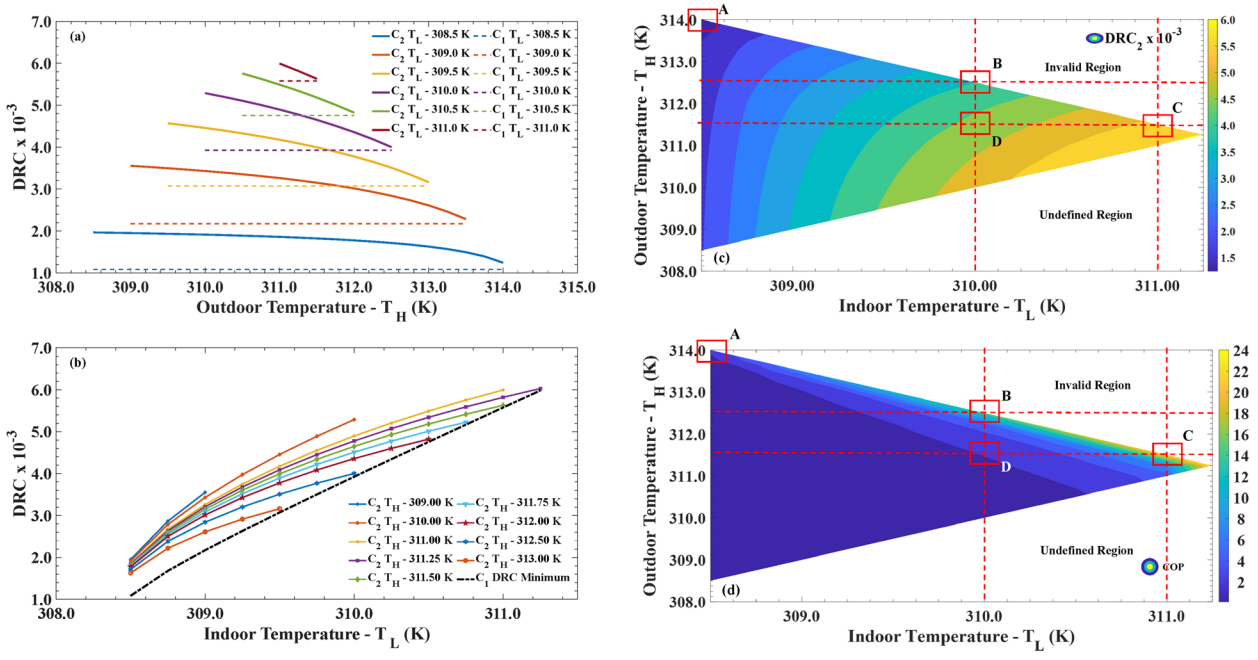

Fig. 5 DRC_2 variation with outdoor temperatures (**a**), DRC_2 variation with indoor temperature (**b**), Impact of indoor and outdoor temperature variations on DRC_2 (**c**) and COP_2 (**d**)

Table 3 Indoor-outdoor temperature combinations for selected cases

Case name	Indoor Temperature (K)—T_L	Outdoor Temperature (K)—T_H
Case A	308.50	314.00
Case B	310.00	312.50
Case C	311.00	311.50
Case D	310.00	311.50

when T_L approaches closely or exceeds T_H. The upper-right region labelled "Invalid Region" indicates that $(NA)_2CuBr_4$ is unsuitable for the Brayton refrigeration cycle under these conditions, as the temperature span between the heat sink and heat source (T_H -T_L) is too large for $(NA)_2CuBr_4$ to achieve cooling.

Figure 5c illustrates that, for Case A, DRC_2 is 3.2 and 4.5 times lower than in Case B and Case C, respectively. This suggests an inverse relationship between the temperature span (ΔT) and DRC_2. When analysing various cases like A, B, and C, the impact of temperature spans on heat transfer time during barocaloric processes in indoor and outdoor conditions is evident. Notably, DRC_2 cannot reach its maximum potential at lower indoor temperatures and higher outdoor temperatures. Thus, to enhance refrigeration capacity, adjustments are required: increasing the duration of the endothermic process (t_2), decreasing the duration of the exothermic process (t_1) and optimising the operational points, such as compression and expansion temperature, are recommended. Optimisation analysis of the reversible Brayton barocaloric refrigeration cycle shows that the DRC_1 remains unchanged (Fig. 3a) regardless of outdoor temperature variations, and the minimum DRC_1 required to operate the refrigeration cycle is also achieved (Fig. 3b) when t_2 equals t_1, denoted as *DRC* minimum in the figures. Since *DRC* is also influenced by (Q_L/Q_H), authors advocate for determining the maximum *COP* first to attain optimal performance within the specified operating temperature range, followed by adjusting the temperature differences of heat transfer in the two isobaric processes to enhance refrigeration capacity.

The response of COP_2 to changes in both indoor and outdoor temperatures is demonstrated in Fig. 5d. The COP_2 shows a direct increasing correlation with both indoor and outdoor temperatures. The temperature difference between the hot and cold reservoirs influences the COP_2. If the indoor temperature increases and the outdoor temperature remains constant, likewise, if the outdoor temperature increases while the indoor temperature stays constant, the temperature difference will decrease, leading to an increase in *COP*. This results in a *COP* of 22.3, 15.2, and 2.65 for the following cases: Case C with a 0.5 K temperature difference, Case B with a 2.5 K difference, and Case A with a 5.5 K difference between indoor and outdoor temperatures.

Case C, Case B, and Case A demonstrate exergy efficiencies $(exergy = (COP_{case}/COP_{max}) \times 100)$ of 52.8%, 36%, and 6.3%, respectively, when compared to the efficiency of a reverse Carnot cycle for NA_2CuBr_4. For

alternative cooling technologies, the maximum exergy efficiencies are reported as follows: desiccant cooling (7%), evaporative cooling (19%), triple-effect absorption cycle (23%), hydraulic refrigeration (25%), Stirling cycle (30%), and thermoelectric cooling (35%). Notably, the exergy efficiencies of Case B and Case C surpass those of all alternative cooling technologies and are comparable to the performance of magnetocaloric refrigeration systems. Additionally, McLinden et al., 2014 conducted a thermodynamic analysis of various refrigerants, including NH_3, R123, R134a, R600a, R32, R22, propane, R-410A, R-1234yf, and R-125, revealed that they exhibit COP values ranging from 6.8 to 8.4 for a simple vapour compression cycle under air-conditioning conditions (evaporator temperature of 283 K and condenser temperature of 313 K) [26]. These results are comparable to the simple cycle analysis; the COP exceeded 5 for evaporator temperatures between 310 K and 311.25 K and condenser temperatures between 311 and 314 K, reaching a peak value of 22.3 at an evaporator temperature of 311 K and a condenser temperature of 311.5 K. Consequently, the *COP* values of the simple reversible barocaloric refrigeration cycle underscore its significant potential for further exploration and optimisation in the context of irreversible barocaloric refrigeration cycles.

3.3 The impact of operational point

This section discusses the COP_1 and DRC_1 of the ideal Barocaloric refrigeration cycle under two cases, A and B, which involve combinations of indoor and outdoor temperature conditions at various compression and expansion operational points. The compression point refers to the temperature of $(NA)_2CuBr_4$ after the material absorbs heat from the indoor environment (point a). At the same time, the expansion point refers to the temperature of the material after the heat rejection process (point c). These compression and expansion points are crucial to optimising the barocaloric system for high performance. Case A was selected for its ability to achieve a high-temperature span, cooling the material by 5.5 K, while Case B represented a general midpoint temperature span difference for the cooling application of this ideal refrigeration cycle.

3.3.1 Effect of operational point temperature range on COP

Figure 6a illustrates the *COP* variation with compression temperatures under selected expansion temperatures for Case A, while Fig. 6b shows the COP_1 variation with expansion temperatures under selected compression temperatures for Case A. Similarly, Fig. 6d and e present the corresponding variations for Case B. Due to the limitations of two-dimensional representations in capturing all operational conditions, three-dimensional plots were generated. These figures illustrate the complete range of compression and expansion temperatures, enabling full utilisation of the material's cooling temperature span resulting from phase change. Figure 6c and f show the COP_1 performance at all operational points for Cases A and B, respectively.

Section 3.2 demonstrates that the *COP* and *DRC* are derived from the ideal barocaloric refrigeration cycle and can be optimised by adjusting the indoor and outdoor temperatures within the specified operating range. For example, consider the operating temperature ranges of Case A ($T_H = 314.0\ K$, $T_L = 308.5\ K$) and Case B ($T_H = 312.5\ K$, $T_L = 310.0\ K$). Case A's *COP* shows significant improvement, increasing by a factor of two to four across a wide range of operational temperatures, achieving a 5.5 K cooling span. It consistently rises from 2.65, as highlighted in Sect. 3.2, to values between 5 and 10. Similarly, Case B's *COP* demonstrates notable improvement, increasing from 15.2 to a peak of 20 within a reasonable range of operational temperatures, with a 2.5 K cooling span.

Figure 6c, f illustrates the distribution of COP_1 influenced by the compression operational point temperature (T_a) and expansion operational point temperature (T_c). The white region represents an invalid region where the barocaloric system would not operate if any combination of material temperatures were selected for the compression or expansion process in the reversible Brayton refrigeration cycle. The figures indicate that COP_1 consistently reaches higher values when the compression temperature point (T_a) is farther from the indoor temperature (T_L) and the expansion temperature point (T_c) is closer to the outdoor temperature (T_H). The reason for this is that when T_a is farther from the indoor temperature, the amount of compression work (W) required by the barocaloric device decreases, resulting in improved system performance. Both Case A and Case B show that *COP* is inversely proportional to the expansion temperature at a constant compression point and inversely proportional to the compression temperature at a constant expansion point. However, comparing Case A and Case B shows that a higher *COP* is observed in Case B due to the higher indoor and lower outdoor operating conditions. In Case B, the lower outdoor temperature enhances heat transfer from the material to the outdoor (Q_H) compared to Case A, as the compression and expansion times are the same. Similarly, the higher indoor temperature facilitates greater energy absorption (Q_L) due to the significant temperature difference between the material and the indoor environment. Therefore, to achieve maximum efficiency, a potential barocaloric cooling device should perform compression at the highest possible material temperature during the endothermic process and expansion at the lowest material temperature during the exothermic process, corresponding to the completion of the

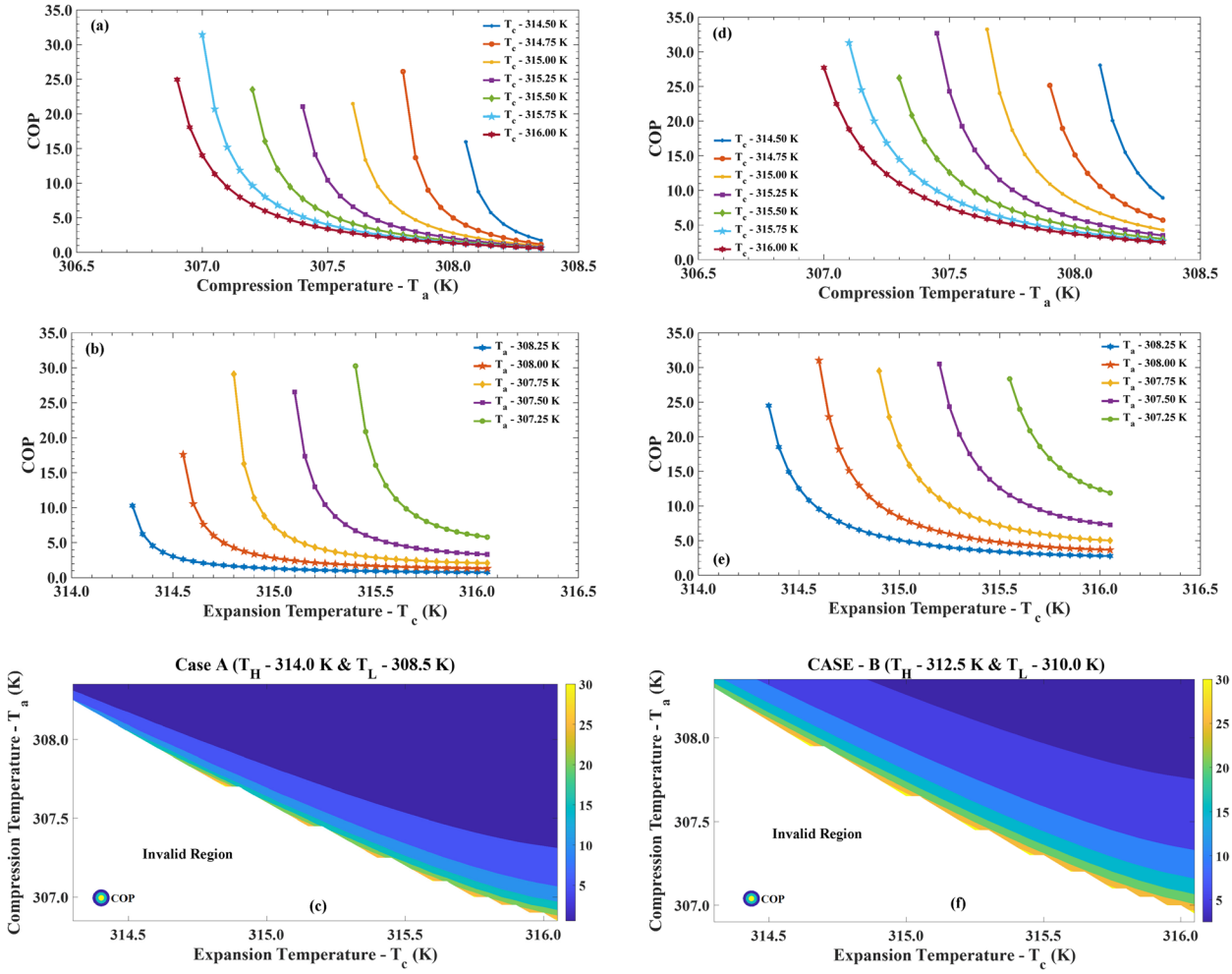

Fig. 6 **a** COP_1 variation with compression temperatures under selected expansion temperatures for Case A. **b** COP_1 variation with expansion temperatures under selected compression temperatures for Case A. **c** COP_1 variation with all compression and expansion temperatures for Case A. **d** COP_1 variation with compression temperatures under selected expansion temperatures for Case B. **e** COP_1 variation with expansion temperatures under selected compression temperatures for Case B. **f** COP_1 variation with all compression and expansion temperatures for Case B

material's phase-change process, irrespective of indoor and outdoor temperature.

3.3.2 Effect of operational point temperature on DRC

Figure 7c and f display *DRC* variation at all operational points for both Cases A and B. As two-dimensional plots could not capture the full range, three-dimensional figures were used to illustrate the complete compression and expansion temperatures, fully utilising the material's cooling temperature span. For Case A, the variation of DRC with compression temperatures at selected expansion temperatures is shown in Fig. 7a, whereas the variation of DRC_1 with expansion temperatures at selected compression temperatures is presented in Fig. 7b. Similarly, Fig. 7d and e illustrate these respective variations for Case B.

The figures display that *DRC* always increases with T_c and decreases with T_a, irrespective of heat reservoir temperatures. From a material perspective, a higher T_c indicates fewer molecules undergoing structural changes by releasing energy outdoors, resulting in shorter time requirements and demonstrating a higher *DRC*. Conversely, a higher T_a suggests that more molecules absorb indoor energy over a longer period, leading to a decrease in *DRC*. Another scenario is that as the expansion temperature point (T_c) increases, the time required to reach that temperature also increases since it is closer to the outdoor temperature. Consequently, the time required for the exothermic process (t_1) increases. Given that the times for the exothermic process and the endothermic process are equal ($t_2 = t_1$) in this scenario, heat absorption (Q_L) will be higher, leading to a higher *DRC*. However, an increase in the compression temperature point means it is much closer to the indoor temperature, resulting in smaller heat absorption and, consequently, a lower *DRC*.

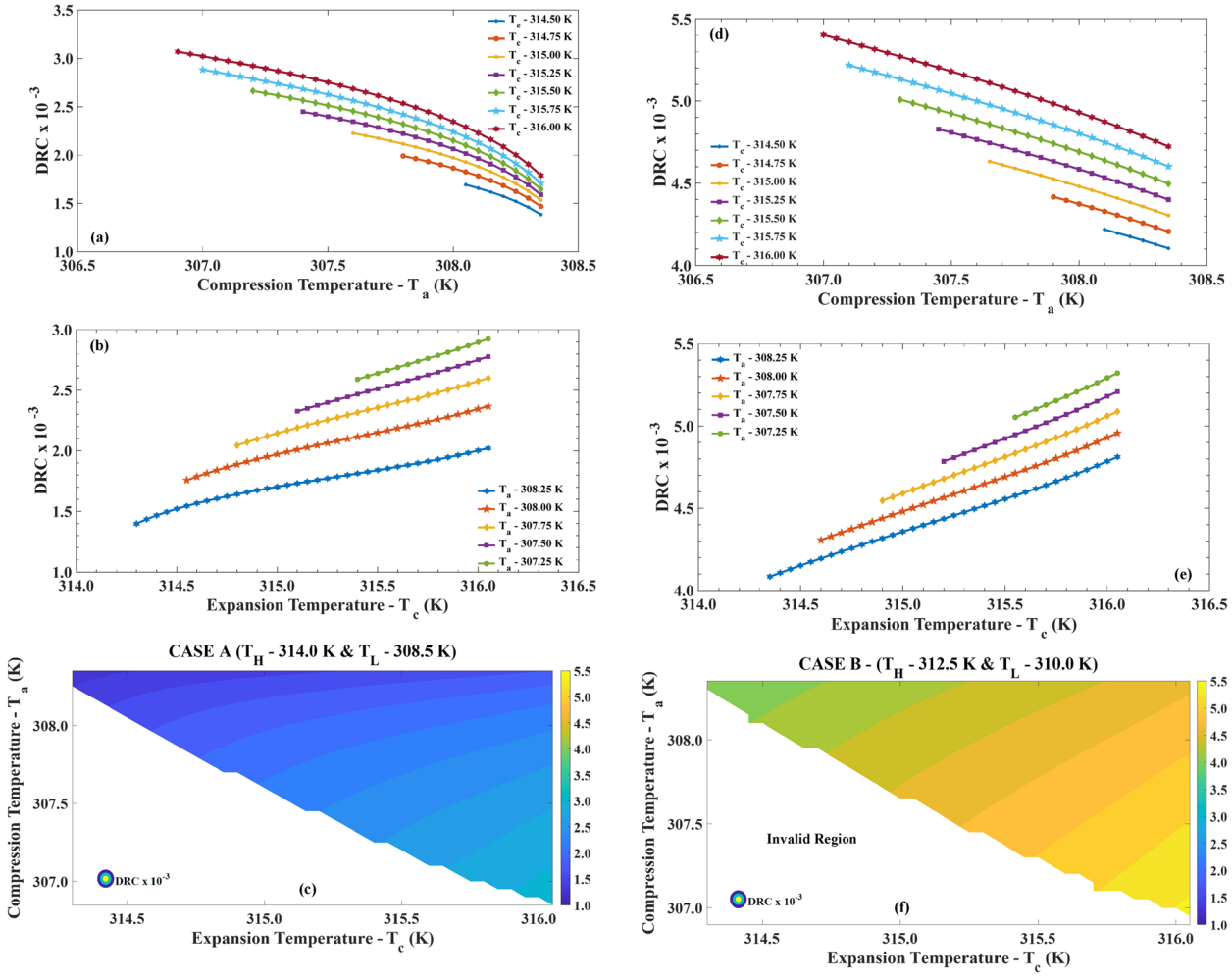

Fig. 7 **a** DRC_1 variation with compression temperatures under selected expansion temperatures for Case A. **b** DRC_1 variation with compression temperatures under selected compression temperatures for Case A. **c** DRC_1 variation with all compression and expansion temperatures for Case A. **d** DRC_1 variation with compression temperatures under selected expansion temperatures for Case B. **e** DRC_1 variation with expansion temperatures under selected compression temperatures for Case B. **f** DRC_1 variation with all compression and expansion temperatures for Case A (**a**) and Case B (**b**)

Compared to Case A, the temperature difference during the heat transfer in the exothermic and endothermic processes for Case B was significantly larger. Consequently, the total time required for heat rejection and absorption is shortened, leading to a relatively higher *DRC*. Therefore, the influence of heat transfer time on the system cannot be overlooked, given the significant temperature difference during heat transfer. Optimising the time ratio between heat rejection and absorption is crucial for system efficiency and is discussed in Sect. 3.5.

The optimisation of the operational point in this simple Barocaloric cycle demonstrates that the *DRC* for Case A can be significantly increased from 1.084×10^{-3}, as presented in Sect. 3.2, to a maximum of 3.025×10^{-3}, achieving a cooling span of 5.5 K. Similarly, Case B showed an increase from 3.926×10^{-3} to 5.469×10^{-3} with a cooling span of 2.5 K. These improvements are crucial, as the *COP* also increased from 15.2 to 22.66 for Case B and from 2.65 to 16.86 for Case A. However, the overall mechanical operation of the device could present a slight drawback, as the compression and expansion processes must operate at a rapid speed within a very short time cycle. Achieving this short-time cycle operation could become a realistic option with sophisticated technological advancements in the Barocaloric refrigeration system. However, developing this system at a laboratory scale to demonstrate proof of concept may not be feasible at present. Therefore, an expansion operational point of 314.3 K and a compression operational point of 308.35 K were selected for further sections to analyse the cooling performance of the reversible/ideal and irreversible barocaloric refrigeration cycle. This selection aims to achieve a broader cooling temperature span and allow the material to undergo exothermic and endothermic processes for the maximum possible duration.

3.4 The impact of work process efficiency on COP

In this section, the adiabatic compression and expansion processes' efficiencies are considered equal, with both referred to by the term work process efficiency, as both are executed using the same barocaloric cooling apparatus and the same piston-cylinder assembly to achieve the desired thermodynamic process. This section investigates the system's performance under various work process efficiencies in an irreversible Brayton Barocaloric refrigeration cycle operating at 500 Bar, with an outdoor temperature of 311.5 K (T_H). In this case, the heat transfer time between heat reservoirs is assumed to be equal for performance analysis under different indoor temperature conditions. However, due to the irreversible nature of the system, the compressibility during compression (β_1) and expansion (β_2) cannot be assumed to be equal.

Figure 8a and b illustrate that the COP_1 and DRC_1 increase with work process efficiency across all indoor temperatures. This occurs because, at lower efficiencies, more work is required during compression and expansion. This behaviour aligns with the observation that the system approaches the performance of an ideal reversible Brayton refrigeration cycle as work process efficiency nears 1, thereby achieving maximum COP_1 and DRC_1. In the scenario discussed, a work process efficiency of 0.75 is required to cool the indoor temperature by 3 K. However, for the system to operate effectively as a refrigeration system, the COP_1 must exceed 1.0. Specifically, to lower the indoor temperature by 2 K, a minimum work process efficiency of 0.96 is necessary for optimal refrigeration. Nevertheless, a work process efficiency of 0.8 indicates a reasonably efficient barocaloric refrigeration system.

Reduction of work process efficiency drastically reduces the COP_1 performance of an irreversible barocaloric refrigeration cycle. For example, in Case C ($T_L = 311.0\ K$

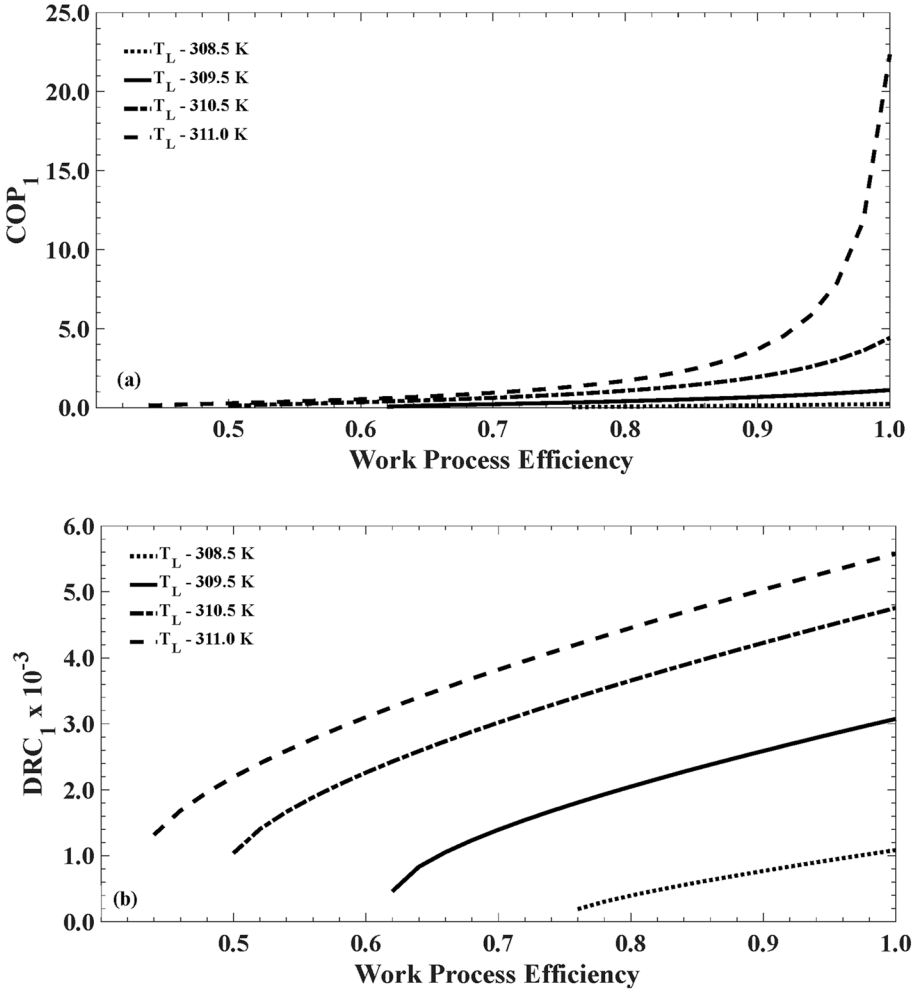

Fig. 8 COP_1 (**a**) and DRC_1 (**b**) variation with work process efficiency at various indoor temperatures

& $T_H = 311.5\ K$), the reverse Carnot cycle efficiency at the selected operational points is 33.8. As shown in Fig. 5d, the cycle can achieve a COP_1 of 22.3 under an ideal Brayton refrigeration cycle. However, the irreversibility of the work process significantly reduces the achievable COP_1 to 3.7 at a work process efficiency of 0.9 and to 1.7 at an efficiency of 0.8, as shown in Fig. 8a, corresponding to exergy efficiencies of 11% and 5%, respectively. Therefore, it is crucial to design an efficient barocaloric piston-cylinder arrangement for the compression and expansion processes when developing a simple barocaloric cooling device.

The typical efficiency range of revolutionised domestic refrigerators, which have undergone a century of technological improvements, usually falls between 2 and 4. In contrast, the case discussed here achieves a *COP* of 1.5 even with a work process efficiency of 0.8. This promising result underscores the potential for further optimisation, paving the way for alternative refrigeration technologies that could eventually rival small-scale vapour compression systems.

3.5 The impact of timing ratio on an irreversible barocaloric refrigeration cycle

3.5.1 Effect of work process efficiency

This section discusses the scenario of Case D ($T_L = 310\ K$ *and* $T_H = 311.5\ K$) as an example under various time ratios (t_r). The time ratio is defined as the proportion of the duration of heat rejection through the heat sink during the exothermic process (t_1) to the duration of heat absorption from the heat source during the endothermic process (t_2). As shown in Fig. 9a, the COP_2 increases exponentially as the time ratio decreases from 1.0, regardless of work process efficiency. However, the time ratio is constrained by the efficiency of the work process in enhancing the COP_2 of the barocaloric system. Reducing the time ratio from 1.0 (equal duration for heat rejection and absorption) to 0.5 (heat absorption time is twice that of heat rejection) at a work process efficiency of 0.8 resulted in an impressive COP_2 increase from 0.67 to 4.09, representing a remarkable 609% improvement. Similarly, COP_2 increased by 326% and 244% for work process efficiencies of 0.7 and 0.6, respectively.

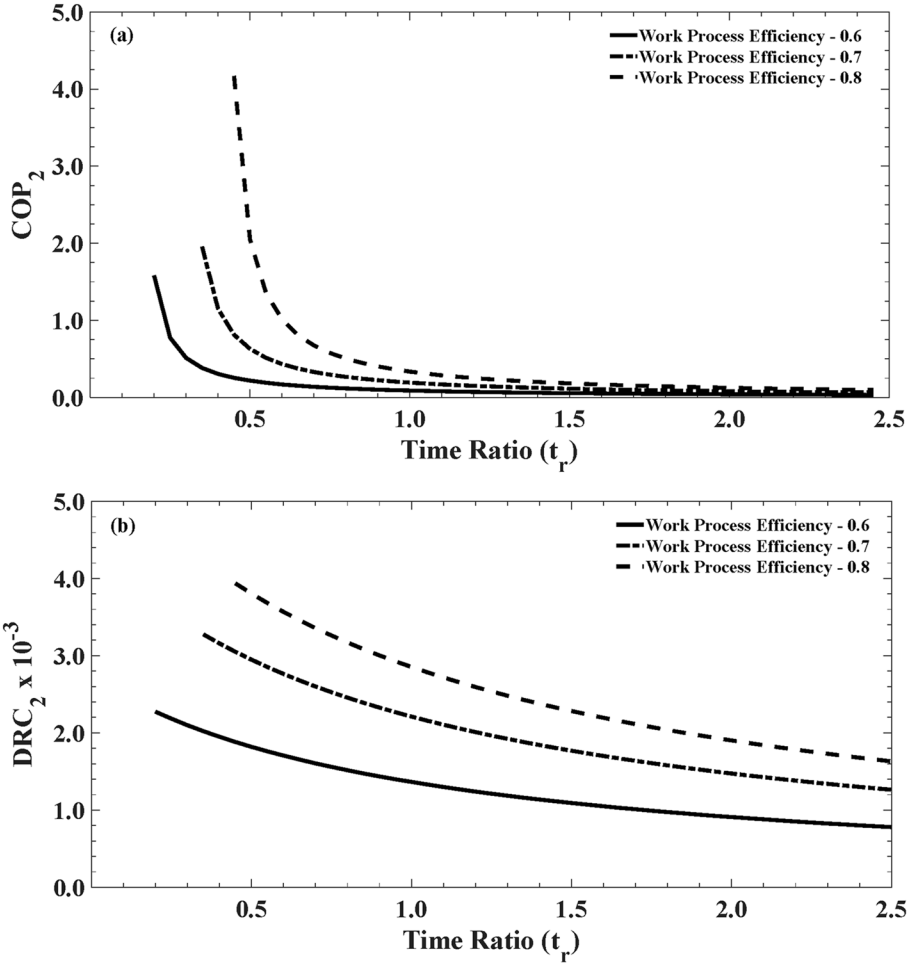

Fig. 9 COP_2 (**a**) and DRC_2 (**b**) variation respect to timing ratio at $T_L = 310$ K & $T_H = 311.5$ K

Figure 9b demonstrates that the DRC_2 increases with the time ratio across the full range of work process analyses. Similarly, the DRC_2 increased by 133% across all work process efficiencies as the time ratio decreased from 1.0 to 0.5. From these analyses, it can be concluded that by developing a barocaloric refrigeration device with reasonable compression and expansion efficiencies, and optimising time ratios, higher *COP* and *DRC* can be achieved. Therefore, analysing other refrigeration systems is essential for selecting the right work process efficiency for further analysis, which is crucial in determining whether a barocaloric refrigeration device can be designed and built in a laboratory setting.

Efficiency losses in vapour compression refrigeration systems arise from friction during the compression and expansion phases, pressure drops during suction and discharge, clearance losses, temperature variations, and refrigerant leakage [27]. Typically, the compression efficiency of vapour compression refrigeration systems is approximately 0.85, accounting for these losses [28].

Caloric cooling technologies, such as magnetocaloric, electrocaloric, and elastocaloric systems, have been developed over many years and share similarities with barocaloric cooling. They undergo significant losses due to material temperature changes and friction within their driving mechanisms. Elastocaloric cooling, in particular, is prone to fatigue loss, which further reduces efficiency. Magnetic refrigeration systems, like barocaloric systems, rely on indirect heat transfer with the external environment. The adiabatic efficiency of the magnetic refrigerator is typically assumed to be between 0.9 and 1.0 [25, 29, 30]. Based on this assumption, Dai et al. [14] conducted a thermodynamic cycle analysis, estimating the compression efficiency for barocaloric refrigeration to be 0.95.

The mechanism of barocaloric cooling systems operates similarly to a hydraulic piston-cylinder arrangement. As with hydraulic systems, the efficiency of barocaloric systems is primarily affected by friction within the piston-cylinder casing and leakage. Additionally, barocaloric systems can experience material fatigue and temperature losses akin to elastocaloric technologies. The typical efficiency of hydraulic pistons ranges from 0.78 to 0.95 [31], depending on the specific design. The approximate experimental value of the work process efficiency for barocaloric systems can only be determined once a device is constructed and tested. For this analysis, the work process efficiency was conservatively estimated at 0.8 for the timing ratio study across various heat source and sink temperatures.

3.5.2 Effect of heat reservoir temperature

Maximising the *COP* and *DRC* of the barocaloric refrigeration system is essential for optimising its performance. Figure 10a, b, and c illustrate the variations in COP_2 and DRC_2 under various heat reservoir temperatures and a work process efficiency of 0.8. The figures show that as the time ratio decreases, COP_2 increases exponentially regardless of the heat reservoir temperature. At the same time, the DRC_2 rises steadily with respect to the heat source temperature. The heat sink temperature does not significantly affect DRC_2. Optimising the time ratio from 1.0 to 0.75 at a work process efficiency of 0.8 resulted in significant improvements. In Case C, the COP_2 increased from 1.7 to 5.2, a 206% improvement, while the DRC_2 rose from 4.45×10^{-3} to 5.09×10^{-3}, a 14.4% increase. Case B saw the COP_2 improve from 1.14 to 2.45, a 115% increase and Case D's COP_2 increased from 0.67 to 1.16, a 73% improvement, as shown in Fig. 10b and a, respectively.

It can be concluded that reducing the exothermic time relative to the endothermic time will enhance the system's performance. Therefore, a barocaloric refrigeration device should be designed and operated such that the heat rejection process time is shorter than the heat absorption process time during the isobaric process. However, optimising the time ratio is constrained by the heat source and heat sink temperatures. Thus, designing and building a smart barocaloric refrigeration device that adjusts the duration of isobaric heat absorption and heat rejection based on the heat reservoir temperatures will significantly improve the system's performance.

The Barocaloric cycle demonstrates the potential for an exergy efficiency of 9.7% with a temperature span of 1.5 K at a work process efficiency of 0.8 and a time ratio of 0.5. This performance is further improved to 32.1% exergy efficiency when the work process efficiency is increased from 0.8 to 0.85. Therefore, improving work process efficiency, while simultaneously optimising the time ratio, should be a priority, with additional efforts and resources directed toward designing efficient mechanical devices. Comparing the potential of the Barocaloric refrigeration device to the Electrocaloric refrigeration prototype built in 2017 by Pei's research group at the University of California, the EC prototype showed an exergy efficiency of only 6.1% with a temperature cooling span of 1.4 K [32]. Based on this comparison, it can be concluded that building a Barocaloric refrigeration device based on NA_2CuBr_4 is highly feasible. Therefore, a comprehensive analysis must be conducted to construct an efficient, simple barocaloric device covering a full range of heat reservoir temperatures, operational point temperatures, and time ratio factors. This analysis is crucial for identifying the optimal time ratio that maximises the system's *COP*, *DRC*, and temperature span. By determining these key parameters, the performance of a simple barocaloric refrigeration system can be optimised, ensuring efficient operation under varying conditions. This approach lays the foundation for

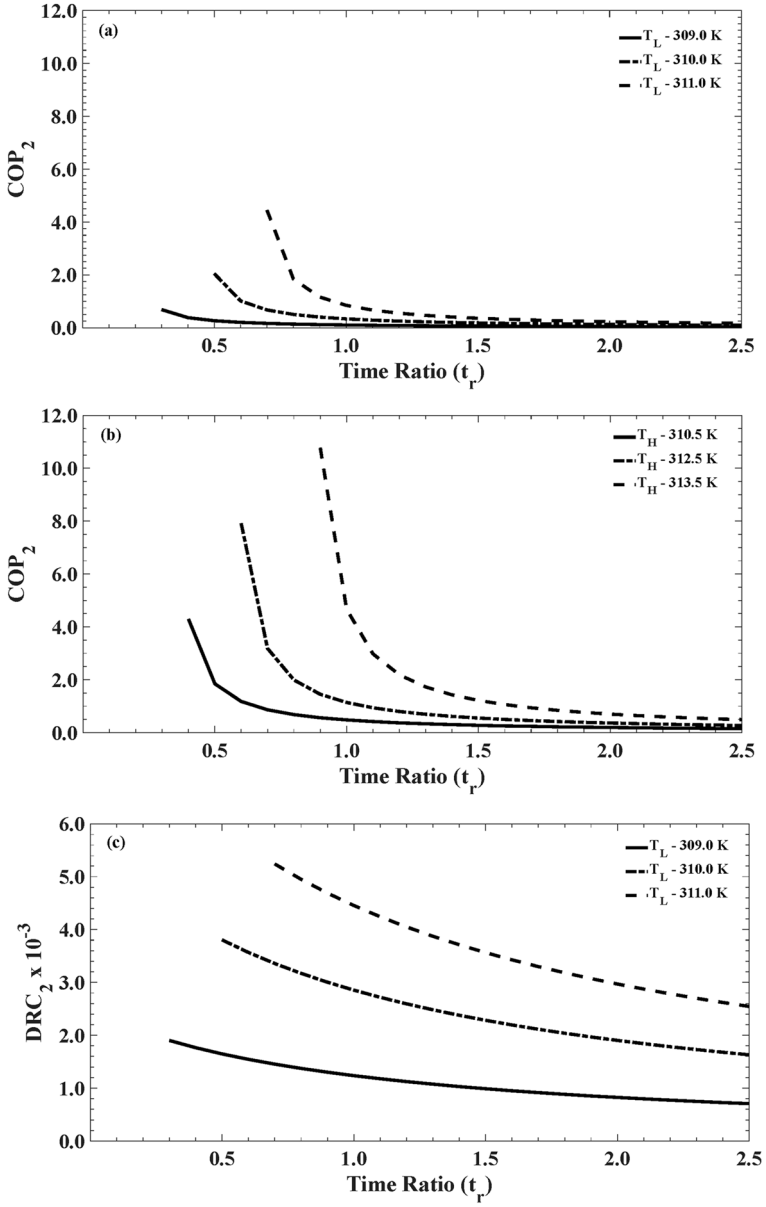

Fig. 10 COP_2 variation with timing ratio at T_H – 311.5 K (**a**), T_L – 310.0 K (**b**), and DRC_2 at T_H – 311.5 K (**c**)

further experimental development, enabling the design of a high-performance barocaloric refrigeration device.

A key limitation of this study is the assumption that compression and expansion efficiencies are equal throughout the barocaloric cycle. It also assumes constant material compressibility during the ideal cycle and variable compressibility during the irreversible cycle, modelled as proportional to the temperature ratio between the start and end points of each compression or expansion phase. However, the actual molecular compressibility under cyclic loading remains unverified. Experimental studies are needed to validate these assumptions and accurately characterise the material's thermomechanical behaviour. Future research should focus on understanding pressure-dependent material properties under dynamic conditions to inform more realistic models. Additionally, the assumed work process efficiency must be confirmed through physical testing. Developing and evaluating a prototype system will be crucial in refining the simulation model and enhancing its alignment with experimental results.

4 Conclusions

This paper evaluates the performance of a barocaloric system using $(NA)_2CuBr_4$ as the refrigerant. Reversible and irreversible Brayton refrigeration cycles are analysed under various operating conditions to identify optimal

system performance, and the following conclusions are reached.

1. The barocaloric system requires a minimum operating pressure of 148 MPa for refrigeration, and its *DRC* performance improves with increasing pressure. The maximum temperature span occurs in the phase transition region at 500 Bar, making it a suitable operating pressure for a barocaloric device.
2. A simple barocaloric refrigeration device, designed and operated with optimised time ratios, can achieve a maximum temperature span of 5.5 K and a *COP* of 5.6, significantly exceeding the typical performance of domestic vapour compression refrigeration systems, whose *COP* generally ranges from 2 to 4.
3. A maximum *COP* of 24.1 is achieved under reversible conditions. In contrast, in the irreversible cycle, a *COP* of 10.8, with a temperature span of 3.5 K, is obtained by fully utilising the phase transition region of $(NA)_2CuBr_4$.

This study validates the material's viability for constructing a simple proof-of-concept barocaloric refrigerator and evaluating the performance of the Barocaloric Brayton refrigeration cycle. Future research focuses on comparing materials with $(NA)_2CuBr_4$ to identify optimal candidates and develop more efficient proof-of-concept devices. Construction and testing of a simple barocaloric device could advance energy-efficient cooling systems and environmentally friendly alternative refrigeration solutions.

Acknowledgements
This research is supported by an Australian Government International Research Training Program (IRTP) Scholarship and the NSW Space Research Network grant "Caloric heat management space technology—Stage I.

Authors' contributions
Pravinth Balthazar: Conceptualisation, Methodology, Writing—Original paper, Programming, Visualisation, Analysis, Data preparation, and prepared figures. Mohammad S. Islam: Supervision, Writing- Reviewing and Editing. Nick S. Bennett: Resources, Writing- Reviewing and Editing, Supervision, Funding acquisition, Project administration.

Funding
Open Access funding enabled and organized by CAUL and its Member Institutions.

Data availability
The data supporting the findings of this study are available from the corresponding author upon reasonable request.

Declarations

Competing interests
The authors declare that there are no conflicts of interest.

Received: 26 January 2026 / Accepted: 25 April 2026
Published online: 18 May 2026

References

1. Zaki, O. M., & Abdelaziz, O. (2024). Critical assessment of R410A alternatives for mini-split air conditioners in the Egyptian market. *Energy and Built Environment, 5*(3), 426–445. https://doi.org/10.1016/j.enbenv.2023.01.003
2. Balthazar, P., Ismail, M. A., Wahab, A. A., Mamat, H., Ramdan, M. I., & Yu, K. H. (2021). Experimental study of desorption and regeneration analysis of cylindrical desiccant layer arrangements. *Journal of Mechanical Science and Technology, 35*(12), 5713–5722. https://doi.org/10.1007/s12206-021-1140-9
3. Coulomb, D., Dupont, J.-L., & Morlet, V. (2017). The impact of the refrigeration sector on climate change - 35. Informatory Note on Refrigeration Technologies. Paris (France). Available: https://inis.iaea.org/Search/search.aspx?orig_q=RN:51010282. Accessed: Jan. 17, 2024.
4. Brown, J. S., & Domanski, P. A. (2014). Review of alternative cooling technologies. *Applied Thermal Engineering, 64*(1–2), 252–262. https://doi.org/10.1016/j.applthermaleng.2013.12.014
5. Aprea, C., Greco, A., Maiorino, A., & Masselli, C. (2019). Is barocaloric an eco-friendly technology? A TEWI comparison with vapor compression under different operation modes. *Climate*, *7*(9). https://doi.org/10.3390/cli7090115
6. Lloveras, P., et al. (2019). Colossal barocaloric effects near room temperature in plastic crystals of neopentylglycol. *Nature Communications, 10*(1), 1803. https://doi.org/10.1038/s41467-019-09730-9
7. Aznar, A., et al. (2020). Reversible and irreversible colossal barocaloric effects in plastic crystals. *Journal of Materials Chemistry A, 8*(2), 639–647. https://doi.org/10.1039/C9TA10947A
8. Seo, J., et al. (2022). Colossal barocaloric effects with ultralow hysteresis in two-dimensional metal–halide perovskites. *Nature Communications, 13*(1), 2536. https://doi.org/10.1038/s41467-022-29800-9
9. Zhang, Y., Shan, K., Li, X., Li, H., & Wang, S. (2023). Research and technologies for next-generation high-temperature data centers – State-of-the-arts and future perspectives. *Renewable and Sustainable Energy Reviews, 171*, 112991. https://doi.org/10.1016/j.rser.2022.112991
10. Kitanovski, A., Plaznik, U., Tomc, U., & Poredoš, A. (2015). Present and future caloric refrigeration and heat-pump technologies. *International Journal of Refrigeration, 57*, 288–298. https://doi.org/10.1016/j.ijrefrig.2015.06.008
11. Qian, S., et al. (2016). A review of elastocaloric cooling: Materials, cycles and system integrations. *International Journal of Refrigeration, 64*, 1–19. https://doi.org/10.1016/j.ijrefrig.2015.12.001
12. Lloveras, P., & Tamarit, J.-L. (2021). Advances and obstacles in pressure-driven solid-state cooling: A review of barocaloric materials. *MRS Energy & Sustainability, 8*, 3–15. https://doi.org/10.1557/s43581-020-00002-4
13. Cirillo, L., Greco, A., & Masselli, C. (2022). Cooling through barocaloric effect: A review of the state of the art up to 2022. *Thermal Science and Engineering Progress, 33*, 101380. https://doi.org/10.1016/j.tsep.2022.101380
14. Dai, Z., She, X., Wang, C., Ding, Y., Zhang, X., & Zhao, D. (2023). Thermodynamic analysis on the performance of barocaloric refrigeration systems using Neopentyl Glycol as the refrigerant. *Journal of Thermal Science, 32*(3), 1063–1073. https://doi.org/10.1007/s11630-023-1801-3
15. Dai, Z., et al. (2024). Dynamic simulation and performance analysis of a solid-state barocaloric refrigeration system. *Energy, 294*, 130800. https://doi.org/10.1016/j.energy.2024.130800
16. Zhu, L., et al. (2023). Barocaloric material with high thermal conductivity for room-temperature refrigeration. *Journal of Thermal Science, 32*(6), 2115–2125. https://doi.org/10.1007/s11630-023-1867-y
17. Dai, Z., et al. (2024). Plastic crystal Neopentyl Glycol/Multiwall Carbon Nanotubes composites for highly efficient barocaloric refrigeration system. *Journal of Thermal Science, 33*(1), 383–393. https://doi.org/10.1007/s11630-023-1891-y
18. Qian, K., et al. (2024). Highly efficient mechanocaloric cooling using colossal barocaloric plastic crystals. *Cell Reports Physical Science, 5*(6), 101981. https://doi.org/10.1016/j.xcrp.2024.101981
19. Stern-Taulats, E., et al. (2015). Reversible adiabatic temperature changes at the magnetocaloric and barocaloric effects in Fe49Rh51. *Applied Physics Letters*, *107*(15). https://doi.org/10.1063/1.4933409
20. Gottschall, T., Stern-Taulats, E., Mañosa, L., Planes, A., Skokov, K. P., & Gutfleisch, O. (2017). Reversibility of minor hysteresis loops in magnetocaloric Heusler alloys. *Applied Physics Letters*, *110*(22). https://doi.org/10.1063/1.4984797
21. Chen, C.-K., & Su, Y.-F. (2005). Exergetic efficiency optimization for an irreversible Brayton refrigeration cycle. *International Journal of Thermal Sciences, 44*(3), 303–310. https://doi.org/10.1016/j.ijthermalsci.2004.09.003
22. Cheng, C.-Y., & Chen, C.-K. (1999). Ecological optimization of an irreversible Brayton heat engine. *Journal of Physics D: Applied Physics, 32*(3), 350–357. https://doi.org/10.1088/0022-3727/32/3/024

23. Roco, J. M. M., Velasco, S., Medina, A., & Hernández, A. C. (1997). Optimum performance of a regenerative Brayton thermal cycle. *Journal of Applied Physics, 82*(6), 2735–2741. https://doi.org/10.1063/1.366104
24. Yang, Z., Xu, Z., Wang, J., Li, Y., Lin, G., & Chen, J. (2020). Thermoeconomic performance optimization of an irreversible Brayton refrigeration cycle using Gd, Gd0.95Dy0.05 or Gd0.95Er0.05 as the working substance. *Journal of Magnetism and Magnetic Materials, 499*, 166189. https://doi.org/10.1016/j.jmmm.2019.166189
25. Xia, Z., Zhang, Y., Chen, J., & Lin, G. (2008). Performance analysis and parametric optimal criteria of an irreversible magnetic Brayton-refrigerator. *Applied Energy, 85*(2–3), 159–170. https://doi.org/10.1016/j.apenergy.2007.04.007
26. McLinden, M. O., Kazakov, A. F., Brown, J. S., & Domanski, P. A. (2014). A thermodynamic analysis of refrigerants: Possibilities and tradeoffs for Low-GWP refrigerants. *International Journal of Refrigeration, 38*, 80–92. https://doi.org/10.1016/j.ijrefrig.2013.09.032
27. Bell, I. H., Groll, E. A., & Braun, J. E. (2011). Performance of vapor compression systems with compressor oil flooding and regeneration. *International Journal of Refrigeration, 34*(1), 225–233. https://doi.org/10.1016/j.ijrefrig.2010.09.004
28. She, X., Yin, Y., & Zhang, X. (2014). A proposed subcooling method for vapor compression refrigeration cycle based on expansion power recovery. *International Journal of Refrigeration, 43*, 50–61. https://doi.org/10.1016/j.ijrefrig.2014.03.008
29. Diguet, G., Lin, G., & Chen, J. (2012). Performance characteristics of an irreversible regenerative magnetic Brayton refrigeration cycle using Gd0.74Tb0.26 as the working substance. *Cryogenics, 52*(10), 500–504. https://doi.org/10.1016/j.cryogenics.2012.05.020
30. Tong, X., Liu. Z., Shen, L., & Chen, H. (2022). Performance investigation and optimization of the magnetic refrigeration cycle with two-stage magnetization and demagnetization. *Energy Conversion and Management*, *254*. https://doi.org/10.1016/j.enconman.2022.115279
31. Saheban Alahadi, M. J., Shirneshan, A., & Kolahdoozan, M. (2017). Experimental investigation of the effect of grooves cut over the piston surface on the volumetric efficiency of a radial hydraulic piston pump. *International Journal of Fluid Power, 18*(3), 181–187. https://doi.org/10.1080/14399776.2017.1337440
32. Ma, R., et al. (2017). Highly efficient electrocaloric cooling with electrostatic actuation. *Science, 357*(6356), 1130–1134. https://doi.org/10.1126/science.aan5980

Publisher's Note